

AIR FORCE INST OF TECH WRIGHT-PATTERSON AFB OH SCHOO--ETC F/6 11/4
MATERIAL DAMPING AS A MEANS OF QUANTIFYING FATIGUE DAMAGE IN CO--ETC(U)
DEC 78 C A BOURNE
AFIT/6A/AA/78D-2
NL

NEL

104

END
DATE
FILMED
4-80
PTIC

AFIT/GA/AA/78D-2

MATERIAL DAMPING AS A MEANS OF
QUANTIFYING FATIGUE DAMAGE
IN COMPOSITES

Thesis

AFIT/GA/AA/78D-2 ✓ Cynthia A. Bourne
2nd Lt USAF

1
RECEIVED
JAN 11 1979
A

Approved for public release; distribution unlimited

MATERIAL DAMPING
AS A MEANS OF
QUANTIFYING FATIGUE DAMAGE
IN COMPOSITES,

Thesis

Presented to the Faculty of the School of Engineering
of the Air Force Institute of Technology

Air University (ATC)

In Partial Fulfillment of the
Requirement for the Degree of

Master of Science

by

Cynthia A. Bourne

Second Lieutenant USAF

Graduate Astronautical Engineering

December 1978

Approved for public release; distribution unlimited.

Accession For	
NTIS GRA&I	<input checked="" type="checkbox"/>
DDC TAB	<input type="checkbox"/>
Unannounced	<input type="checkbox"/>
Justification	<input type="checkbox"/>
By	
Date	
Initials	
Signature	

A

0122-5

1B

Preface

It is suggested that debonding and fiber fracture in composite materials might lead to significant internal energy losses. In the past, this damage has been assessed primarily by nondestructive techniques such as ultrasonics and radiography. This was an experimental study to test the feasibility of using the measurement of internal energy loss as a nondestructive technique to determine the amount of damage that has occurred in a composite during a fatigue test. I performed fatigue tests on graphite-epoxy composite specimens in order to quantify the damage in terms of the damping characteristics of the composite.

I am indebted to Dr. George Sendeckyj of the Air Force Flight Dynamics Laboratory for his support and assistance in providing the specimens required for this investigation; to Ed Porter and Ron Selner of the Air Force Materials Laboratory for performing damage inspection through radiography and ultrasonics.

I am most appreciative of Capt. Daniel Hayes, AFIT Mechanics Laboratory Engineer, for his invaluable technical assistance and support. I am deeply grateful to Dr. Peter Torvik, my thesis advisor, who provided guidance and encouragement throughout this study.

To Gary Andreoletti, I offer my thanks for his patience and understanding throughout this study.

Cynthia A. Bourne

Contents

	<u>Page</u>
Preface	11
List of Figures	iv
List of Tables	v
Symbols	vi
Abstract	vii
I. Introduction	1
II. Analysis of Beam Stress and Displacement	4
III. Experimental Procedures	17
Specimen Description	17
Constant Amplitude Cycles	17
Logarithmic Decrement	22
Bandwidth	22
NDT	24
IV. Results and Discussion	27
Bending Fatigue Tests	27
Damping	27
Frequency	41
V. Conclusions	45
Bibliography	46
Appendix A	48
Appendix B	53
Appendix C	55
Vita	56

List of Figures

<u>Figure</u>		<u>Page</u>
1	Bending Moment, Shear Force, and Axis Directions	5
2	Specimen Geometry	18
3	Schematic of Vibration	20
4	Beam Mounted on Vibration Exciter Head	21
5	Trace of Damped Free Vibration	23
6	Bandwidth Curve	25
7	S-N Plot	29
8	X-ray of Typical Damage	30
9	Ultrasonic C-Scan of Typical Damage	31
10	η -N Plot, Constant Maximum Stress	32
11	Air Damping Experiment	40
12	η - σ_R Plot at 10^4 cycles	42
13	ν_R -N Plot, Typical Values	43
A-1	Moment on Laminate Beam	49
A-2	Geometry of an N-Layered Laminate	49

List of Tables

<u>Table</u>		<u>Page</u>
I.	Material Constants	12
II.	Fatigue Test Results	28
III.	Damping, AB 74	34
IV.	Damping, AB 77	34
V.	Damping, AB 81	35
VI.	Damping, AB 82	35
VII.	Damping, AB 90	36
VIII.	Damping, AB 93	36
IX.	Damping, AB 94	37
X.	Damping, AB 95	37
XI.	Damping, AB 96	38
XII.	Damping, AB 98	38
XIII.	Damping, AB 99	39
XIV.	Natural Frequencies	44
XV.	Static Stiffness	53

Symbols

A	cross-sectional area of beam, in ²
a _T	Maximum tip acceleration, in/sec ²
c	specimen thickness, in
δ _T	maximum tip amplitude, in
E	Young's Modulus, lb/in ²
E ₁ , E ₂	modulus of composite in longitudinal and transverse directions of fiber axes, respectively, lb/in ²
EI	stiffness, lb-in
G ₁₂	shear modulus in x-y plane, lb/in ²
g	gravitational acceleration, ft/sec ²
l	effective beam length from root to tip, in
I	moment of inertia, in ⁴
M	bending moment, lb-in
N	number of cycles
p	frequency of vibration, rad/sec
Q	shear force, lb
x, y, z	coordinate axes and displacements, in, along those axes
η	coefficient of damping
ν _R	resonant frequency, cps
ν ₁₂ , ν ₂₁	Poisson's ratio
ρ	material density, slugs/in ³
σ	stress, lb/in ²
σ _R , σ _{max}	stresses at root and edge of hole, respectively, lb/in ²

Abstract

The purpose of this experimental study was to investigate the possibility of quantifying damage in composites in terms of damping characteristics. Bending fatigue tests were performed on $((0/\pm 45/90)_s)_2$ T300/5208 graphite-epoxy composite specimens. Testing was performed by exciting a cantilever beam so as to maintain a constant amplitude at resonant frequency. Results indicate that the amount of damage occurring in this composite can be explained in terms of an increase in its material damping. The resonant frequency was found to decrease as the material damage increased.

MATERIAL DAMPING AS A MEANS OF QUANTIFYING FATIGUE DAMAGE IN COMPOSITES

I. Introduction

Background

Composite materials are ideal for structural applications where high strength-to-weight and stiffness-to-weight ratios are required. Aircraft and spacecraft are typical weight-sensitive structures in which composite materials are cost-effective.

Composites designated as advanced fiber-reinforced composite materials are those with new ultrahigh strength and stiffness fibers such as boron and graphite. The matrix material can be a plastic such as epoxy or a metal such as aluminum. Advanced composites have two major advantages: improved strength and stiffness.

Composites can be made three times as strong as aluminum yet weigh only 60 percent as much. Other composites can be made that have the same strength and stiffness as high-strength steel, but are 70 percent lighter. Moreover, composite materials can be tailored to efficiently meet design requirements of strength, stiffness, and other parameters. These advantages should lead to new and more efficient aircraft and spacecraft designs in contrast to those based on conventional materials.

The strength of composites is governed by their flaw-initiated characteristics. Thus, the mechanics of fracture including crack propagation or extension are of extreme importance in the design analysis of composite structures. The fracture process takes place in three stages. First, an initial flaw may be present or a microcrack initiated. Second, the microcrack grows and may link with

others to attain microcrack size. Third, at a critical stress level, the crack propagates through the material. Fracture occurs when the crack reaches a critical length.

Salkind (Ref 13) has proposed that composites may fail by matrix cracking, fiber failure, and delamination, either separately or in combination. He also suggests that a fatigue failure criterion could be the number of cycles to a given change in stiffness rather than the number of cycles to fracture since the loss of stiffness can result in structural failure long before complete fracture occurs.

The internal damping of fiber-reinforced composites is more sensitive than stiffness to the failure mechanisms previously mentioned. Accordingly, damping measurements can be valuable in the early detection of structural damage.

Much of the experimental work on the damping and stiffness properties of composite materials has been concerned with measuring frequency and temperature dependence (Ref 4). Both aluminum and fiber-reinforced plastic beams have been tested by the methods of logarithmic decrement and resonant dwell (Ref 8). Air damping was shown to be significant at low frequencies and large amplitudes. Schultz and Tsai (Ref 14) used logarithmic decrement and bandwidth techniques to test aluminum and glass fiber-reinforced plastics in flexural vibration. They found that the amount of fatigue cracking correlated reasonably well with the amount of increase in damping. Ulitchny and Lucas (Ref 10) studied the change in the damping of free vibrations and found crack damage present as changes in damping occurred.

For the commercial utilization of composites, it is necessary to ensure material integrity through reliable methods. Damage

evaluation by nondestructive techniques (NDT) is currently being investigated. Of the NDT methods available, holography and ultrasonics show the most promise. Because damping can be expected to be sensitive to microstructural damage, damping measurements may provide a means of achieving the necessary quality control.

This thesis studied the feasibility of using the change in material damping to quantify structural damage in the course of a destructive bending fatigue test on composite beams. Observed changes in damping were compared with NDT results in order to provide a comparison between their two means of evaluating damage.

II. Analysis of Beam Stress and Displacement

Beam Theory

The composite specimens were modeled as beams and, as such, a few simplifying assumptions have been made:

- 1) Beam deformations are described by the elementary theory of flexure, so that plane sections normal to beam axis remain plane and normal to the deformed axis
- 2) Each ply is assumed to satisfy the linear, elastic constitutive relationship
- 3) Plies are assumed to have uniform thickness

The well-known differential equation of the deflection curve of a beam whose vibrations occur in its plane of symmetry is

$$EI \frac{d^2 y}{dx^2} = -M \quad (1)$$

in which

$y(x)$ = deflection of the neutral axis,

EI = stiffness, and

M = bending moment at any cross-section. The direction of the axis and positive directions of bending moments and shear forces are shown in Figure 1.

Differentiating Eq (1) twice gives

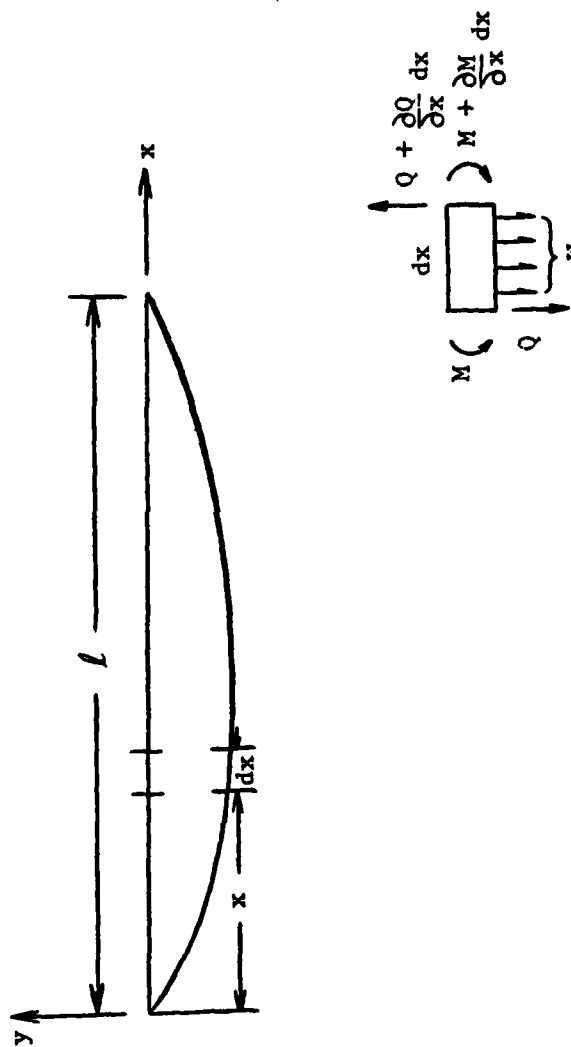


Figure 1. Bending Moment, Shear Force, Axis Directions

$$\frac{d}{dx} EI \left(\frac{d^2 y}{dx^2} \right) = \frac{dM}{dx} = Q \quad \text{and}$$

$$\frac{d^2}{dx^2} EI \left(\frac{d^2 y}{dx^2} \right) = \frac{dQ}{dx} = -w \quad (2)$$

The continuous load of intensity, w , can be expressed as

$$\rho A \frac{\partial^2 y}{\partial t^2} \quad (3)$$

Where ρ is the mass of beam material per unit volume and A is the cross-sectional area.

Letting $w = \rho A \frac{\partial^2 y}{\partial t^2}$ in Eq (2), the general equation for

lateral vibration of a beam becomes

$$\frac{\partial^2}{\partial x^2} EI \frac{\partial^2 y}{\partial x^2} = - \rho A \frac{\partial^2 y}{\partial t^2}$$

When EI remains constant along the length of the beam, this equation becomes

$$EI \frac{\partial^4 y}{\partial x^4} = - \rho A \frac{\partial^2 y}{\partial t^2}$$

or

$$\frac{\partial^2 y}{\partial t^2} + a^2 \frac{\partial^4 y}{\partial x^4} = 0 \quad (4)$$

$$\text{where } a^2 = \frac{EI}{A\rho} \quad (4a)$$

The deflection of a beam at any location varies harmonically

with time and can be expressed as

$$y = X(A \cos pt + B \sin pt) \quad (5)$$

Where X is a function of the coordinate x . Substituting Eq (5) into Eq (4) leads to

$$\frac{d^4 X}{dx^4} = \frac{p^2}{a^2} X \quad (6)$$

$$\text{Using the notation } \frac{p^2}{a^2} = p^2 \frac{\rho A}{EI} = k^4 \quad (7)$$

it can be verified that $\sin kx$, $\cos kx$, $\sinh kx$, and $\cosh kx$ are all solutions of Eq (6) and that the general solution can be written in the form

$$X = C_1(\cos kx + \cosh kx) + C_2(\cos kx - \cosh kx) + C_3(\sin kx + \sinh kx) + C_4(\sin kx - \sinh kx) \quad (8)$$

where C_1 , C_2 , C_3 , and C_4 are constants to be determined from the end conditions of the beam.

Assuming that one end ($x = 0$) is built in and the other end is free, the following end conditions are obtained:

$$(X)_{x=0} = 0 \quad (a)$$

$$\left(\frac{dX}{dx}\right)_{x=0} = 0 \quad (b)$$

$$\left(\frac{d^2 X}{dx^2}\right)_{x=l} = 0 \quad (c)$$

$$\left(\frac{d^3 X}{dx^3}\right)_{x=l} = 0 \quad (d)$$

The first two conditions result in $C_1 = C_3 = 0$. The other two give the following equation from which the frequency can be obtained:

$$(\cos kl)(\cosh kl) = -1$$

When a tip mass is added to the previously free end of the beam, new end conditions are obtained:

$$(X)_{x=0} = 0 \quad (e)$$

$$\left(\frac{dX}{dx}\right)_{x=0} = 0 \quad (f)$$

$$\left(\frac{d^2X}{dx^2}\right)_{x=1} = 0 \quad (g)$$

$$\left(\frac{d^3X}{dx^3}\right)_{x=1} = \frac{m}{EI} X(1)(-p^2) \quad (h)$$

Where m = tip mass. The rotatory inertia of the tip mass has been neglected. Again, the first two conditions give $C_1 = C_3 = 0$ in Eq (8). The last two give the following equation:

$$\frac{(\cos kl)(\cosh kl) + 1}{(\sin kl)(\cosh kl) - (\cos kl)(\sinh kl)} = \frac{p^2 m}{k^3 EI} \quad (9)$$

From Eqs (7) and (4a)

$$p^2 = \frac{EI k^4}{\rho A} \quad (9a)$$

and Eq (9) can be expressed as

$$\frac{(\cos kl)(\cosh kl) + 1}{(\sinh kl)(\cosh kl) - (\cos kl)(\sin hl)} = kl \left(\frac{m}{\rho A l} \right) \quad (9b)$$

This transcendental equation, together with Eq (9a), must be solved in order to find the natural frequencies in terms of the mass ratio of tip mass to beam.

An approximate method known as Rayleigh's Quotient can also be used to estimate the frequency of vibration. Its application comes from consideration of the total energy of the system. In applying this method, an initial assumption has to be made regarding the beam deflection shape during vibration. In this case, the deflection was taken to be

$$X = f(x) = x^2(3l-x) \quad (10)$$

The potential energy of the beam is simply its strain energy:

$$\int_0^l \frac{EI}{2} \left(\frac{d^2 y}{dx^2} \right)^2 dx = \int_0^l \frac{EI}{2} \left(\frac{d^2 X}{dx^2} \right)^2 (\sin pt)^2 dx$$

As the tip mass is assumed to contribute no potential energy, the maximum potential energy is then

$$\int_0^l \frac{EI}{2} \left(\frac{d^2 X}{dx^2} \right)^2 dx \quad (11)$$

The kinetic energy in the beam is

$$\int_0^1 \frac{\rho A}{2} \left(\frac{dy}{dt} \right)^2 dx = \int_0^1 \frac{\rho A p^2 X^2}{2} \cos^2 pt dx$$

This gives a maximum kinetic energy of

$$\int_0^1 \frac{\rho A}{2} p^2 X^2 dx \quad (12)$$

for the beam. The tip mass contributes to the kinetic energy of the system:

$$\frac{m}{2} \left(\frac{dy}{dt} \right)^2 \Big|_{x=1} = \frac{m}{2} \left(p^2 X^2 \right)_{x=1} \cos^2 pt$$

Then the maximum kinetic energy of the tip mass is

$$\frac{m}{2} p^2 X^2 \Big|_{x=1} \quad (13)$$

The total energy of the system is a constant and equal to the sums of the kinetic and potential energies. It follows that the maximum kinetic and potential energies of the system can be equated. This yields:

$$\int_0^1 \frac{EI}{2} \left(\frac{d^2 X}{dx^2} \right)^2 dx = \int_0^1 \frac{\rho A}{2} p^2 X^2 dx + \frac{m}{2} p^2 X^2 \Big|_{x=1}$$

Rearranging, the frequency can be found to be:

$$p^2 = \frac{\int_0^1 \frac{EI}{2} \left(\frac{d^2 X}{dx^2} \right)^2 dx}{\int_0^1 \frac{\rho A X^2}{2} dx + \frac{m}{2} X(1)^2} \quad (14)$$

Substituting Eq (10) into Eq (14) gives the frequency in terms of

the assumed beam deflection:

$$p^2 = \frac{\int_0^1 \frac{EI}{2} (61-6x)^2 dx}{\int_0^1 \frac{\rho A}{2} x^4 (31-x)^2 dx + \left[\frac{m}{2} x^2 (31-x)^2 \right]_{x=1}}$$

carrying out the integration yields

$$p^2 = \frac{210 EI}{33 \rho A l^4 + 70 m l^3} \quad (15)$$

In both Rayleigh's Quotient and the exact solution, p^2 can be solved for in terms of the tip and beam masses. The necessary material constants for the material used in this investigation were determined and are listed in Table I. Eq (9) can be solved for kl by an iterative process and the resonant frequency, ν_R , can be determined from Eq (9a). This yields $p = 174.96$ rad/sec or $\nu_R = 27.85$ cps for exact solution. Using Rayleigh's method, $p = 171.62$ rad/sec or $\nu_R = 27.31$ cps. There is less than two percent error in the frequency determined by both methods.

Root Stress and Tip Amplitude

Since the experimental procedure employed in this investigation used the measurement of tip displacement as a means of controlling beam stress, it was necessary to develop a relationship between stresses and tip displacements. Since the beam was assumed to be in simple bending, nominal beam stresses were taken to be

$$\sigma = \frac{Mc}{I}$$

Incorporating Eqs (1) and (5), the maximum outer fiber stress at any point along the beam is

Table I

Specimen Material Constants

Young's Modulus, E^1	1.138×10^7 psi
Area Moment of Inertia, I	5.1177×10^{-5} in ⁴
Stiffness, EI	5.8233×10^2 lb-in
Beam thickness, $2c$	0.085 in
Beam width, D	1.00 in
Effective beam length from root to tip mass, l	5.12 in
Beam Mass, $\rho A l$	7.734×10^{-4} slugs
Tip Mass, m_T , includes accelero- meter, fiberglass doublers, beam tip beyond center of accelerometer	4.446×10^{-3} slugs
Mass Ratio, $\frac{m_T}{\rho A l}$	5.749

1. Young's Modulus was computed by the method described in Appendix A

$$\sigma = cE \frac{d^2 X}{dx^2} (\text{Acospt} + \text{Bsinpt})$$

The stress at the root ($x=0$) is then

$$\sigma_R = cE \frac{d^2 X(0)}{dx^2} (\text{Acospt} + \text{Bsinpt}) \quad (16)$$

Acceleration of the tip can be expressed as

$$a_T = \frac{d^2 y}{dt^2} = p^2 X(\text{Acospt} + \text{Bsinpt})_{x=1} \quad (17)$$

Since the ratio of root curvature to tip displacement is determined solely by the mode shape, it is convenient to combine Eqs (16) and (17) into

$$\sigma_R = \frac{cE}{p^2} a_T \frac{X''(0)}{X(1)} \quad (18)$$

Using the approximate mode shape, Eq (10), we find

$$\sigma_R = \frac{a_T}{p^2} \frac{cE}{f(1)} \frac{f''(0)}{f(1)} \quad (19)$$

Since the tip amplitude is related to the acceleration through

$$\delta_T = \frac{a_T}{2} \quad (20)$$

the tip amplitude required to produce a desired stress at the root is

$$\delta_T = \frac{\sigma_R}{cE} \frac{f(1)}{f''(0)} = \frac{\sigma_R}{cE} \frac{1}{3} \quad (21)$$

Using the exact mode shape, Eq (8), with $C_1 = C_3 = 0$ and

$$C_2 = \frac{-C_4(\sin kl + \sinh kl)}{\cos kl + \cosh kl} \quad (22)$$

results in

$$X(x) = C_4 \left[(\sin kx - \sinh kl) - \frac{(\sin kl + \sinh kl)(\cos kx - \cosh kx)}{\cos kl + \cosh kl} \right] \quad (23)$$

Thus

$$X(1) = 2C_4 \left[\frac{(\sin kl)(\cosh kl) - (\cos kl)(\sinh kl)}{\cos kl + \cosh kl} \right] \quad (24)$$

and

$$X''(0) = 2C_4 k^2 \left[\frac{\sin kl + \sinh kl}{\cos kl + \cosh kl} \right]$$

Thus

$$\sigma_R = \frac{cE_T}{p^2} k^2 \left[\frac{\sin kl + \sinh kl}{(\sin kl)(\cosh kl) - (\cos kl)(\sinh kl)} \right]$$

For the beams used in this investigation, Eq (9b) was found to yield a value of $kl = .84142$ or

$$\delta_T = \frac{\sigma_R}{cE} \left[\frac{(\sin kl)(\cosh kl) - (\cos kl)(\sinh kl)}{k^2 (\sin kl + \sinh kl)} \right]$$

or

$$\delta_T = .3312 \frac{\sigma_R l^2}{cE}$$

The formula based on the approximate mode shape differs from this by less than one percent.

For a beam having the properties given in Table I,

$$\sigma_R = 55,713 \delta_T \text{ psi/in}$$

Inclusion of a hole centered a distance b from the root leads to stresses at the hole edge (Ref 12) given by

$$\sigma_{\max} = f \frac{6M(b)}{c^2(D-2r)} \quad (25)$$

$$\text{Where } f = \left[1.79 + \frac{.25}{1 + \frac{2r}{c}} + \frac{.81}{1 + \left(\frac{2r}{c}\right)^2} - \frac{.26}{1 + \left(\frac{2r}{c}\right)^3} \right] \times \left[1 - 1.04 \frac{2r}{D} + 1.22 \left(\frac{2r}{D}\right)^2 \right] \quad (26)$$

r = hole radius

D = width of beam

$2c$ = thickness of beam

M = moment at hole = EIy''

The stress at the hole can be expressed in terms of the nominal stress where the nominal stress is

$$\sigma_n = \frac{M(b)c}{I} = \frac{6M(b)}{Dc^2}$$

The stress concentration factor is found to be

$$\frac{\sigma_{\max}}{\sigma_n} = \frac{f}{1 - \frac{2r}{D}} \quad (27)$$

and has a value of 2.0701 for $r=0.098$ in, $D=1.00$ in, and $c=0.085$ in.

The nominal stress can be written in terms of the tip amplitude since

$$M = EIX''(\text{hole})$$

so that

$$M(b) = EI \frac{d^2 X(b)}{dx^2}$$

Substituting the exact mode shape given by Eq (23) and eliminating C_4 through the use of Eq (24), the nominal stress is found to be

$$\sigma_n = Ec \delta_T k^2 \left[\frac{(\text{sinkb}-\text{sinhkb})(\text{coskl}+\text{coshkl})-(\text{sinkl}+\text{sinhkl})}{2[(\text{sinkl})(\text{coshkl})-(\text{coskl})(\text{sinhkl})]} - \frac{(\text{sinkl}+\text{sinhkl})(\text{coskb}-\text{coshkb})}{2[(\text{sinkl})(\text{coshkl})-(\text{coskl})(\text{sinhkl})]} \right]$$

For a beam having the properties in Table I,

$$\sigma_n = 25,089 \delta_T \text{ psi/in}$$

Combining this with the stress concentration factor given by Eq (27), the stress at the edge of the hole is found to be

$$\sigma_{\max} = 52,384 \delta_T \text{ psi/in}$$

where δ_T is the tip displacement. This value is seen to be slightly less than the stress at the root of the beam; however, failure may be expected to initiate at the hole edge because of inter-laminar edge stresses (Ref 14) and imperfections generated by the process of creating the hole.

III. Experimental Procedures

Specimen Description

Twelve specimens with the geometry shown in Figure 2 were supplied by the Air Force Flight Dynamics Laboratory. They were machined from a single 16-ply, Thornel 300/5208, graphite-epoxy panel fabricated by Monsanto Research Corporation. The multiple layers are arranged symmetrically about the middle surface at orientations of 0, 45, -45, 90, 90, -45, 45, 0 degrees to the x-axis starting with the top ply and progressing to the middle surface. These orientations are repeated for the remaining eight plies below the middle surface. This layup can be expressed as $((0/^{+45}/90)_s)_2$. Rectangular fiberglass doublers, .118 inch thick, with one edge beveled at 30 degrees were adhesively bonded to the specimens. A circular hole was drilled in the center of each specimen. Typical dimensions of the specimens were one inch wide, 0.085 inch thick, eight inches long, with a center hole diameter of 0.20 inch. An aluminum beam of the same geometry as the specimens was used to develop the testing procedures as was an unusable specimen, AB 70. After mounting, the effective length of each specimen from root to tip was 5.12 inches as defined in Figure 2.

Constant Amplitude Cycles

Each specimen was taken to failure where failure for this experiment was defined as extensive visual fiber delamination accompanied by a significant change in resonant frequency. Stress levels were chosen so that failure would occur between 10^4 and 10^6 cycles. From

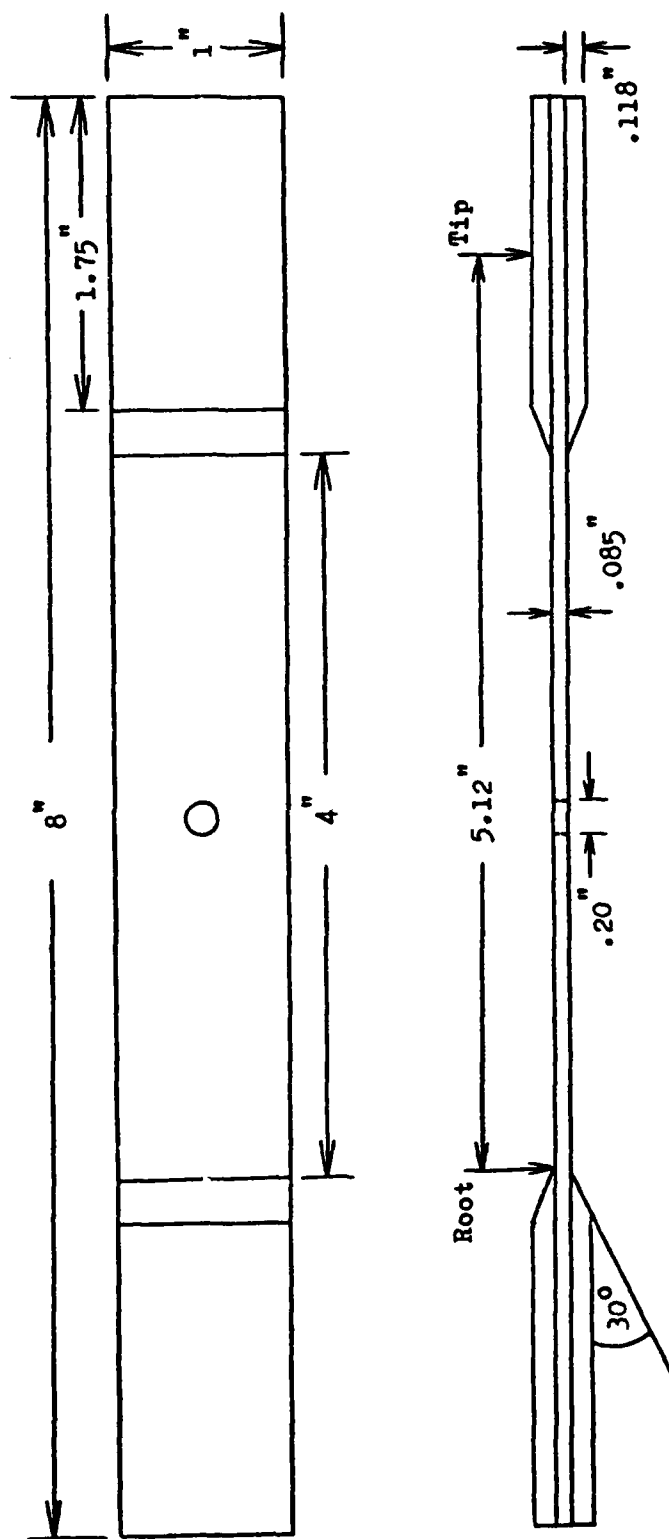


Figure 2. Specimen Geometry

these stresses, corresponding tip amplitudes were calculated from Eq (21). Constant tip amplitude was maintained in order to keep a constant maximum stress at the root of the beam while at resonance. Resonance was found by observing the peaking of beam response with varying excitation frequency on an oscilloscope.

An M-B electrodynamic vibration exciter, model C10E, was used for all tests. As the schematic in Figure 3 shows, it was driven by an M-B automatic vibration exciter control, model N695/696, via an M-B power amplifier. The moving element of the exciter was fitted with an aluminum fixture that served as the mount for each specimen. Figure 4 illustrates this arrangement. An Endevco piezo-electric accelerometer, model 2235C, was glued onto the specimen free end and provided feedback to the control unit through two Endevco preamplifiers, models 2614B and 2621. The control unit integrated the acceleration twice and drove the shaker with a sinusoidal signal so as to shake the specimens vertically and maintain the specimens at constant tip amplitude at resonance. This amplitude was read and monitored directly from the control unit. The same accelerometer and preamplifiers sent a signal to a Tektronix oscilloscope, model 465M, which monitored the free end acceleration. Another accelerometer of the same type was mounted on the aluminum block at the clamped end of the specimens. Its signal was fed into an M-B vibration meter, model N524, from which base displacement was monitored.

A CMC universal counter-timer, model 726C, monitored the driving frequency continuously. Cycles were counted using this resonant frequency for each beam. This frequency and the time of each

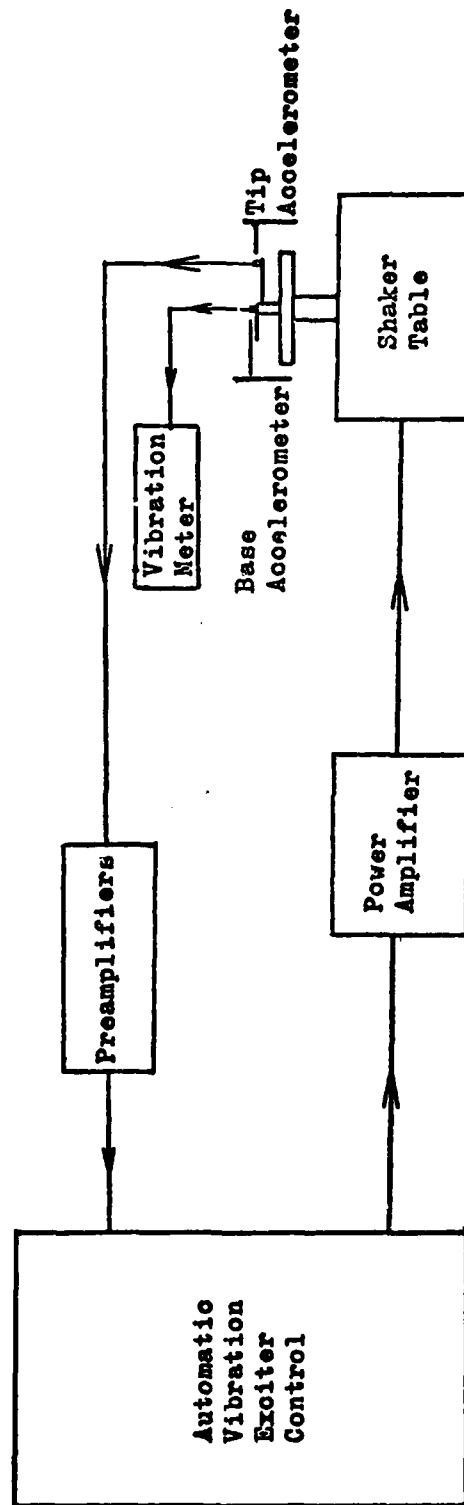


Figure 3. Schematic of Vibration Test System



Figure 4. Beam Mounted on Vibration
Exciter Head

test run were used to determine the number of cycles applied in each specimen.

Twisting was not pronounced enough to be noticed in the system.

Logarithmic Decrement

In a system with $\eta < 1$, the degree of damping can be defined in terms of successive peak values of a tip amplitude as a function of time obtained in free vibration. For any two maxima separated by n cycles of oscillation as shown in Figure 5, the ratio of these two maxima is

$$\frac{x_n}{x_0} = e^{-2\pi\eta n / (1 - \eta^2)^{1/2}}$$

from which η can be expressed as

$$\eta = \left\{ \frac{\left[\frac{\ln \frac{x_n}{x_0}}{-2\pi n} \right]^2}{1 + \left[\frac{\ln \frac{x_n}{x_0}}{-2\pi n} \right]^2} \right\}^{1/2}$$

A Honeywell visicorder, model 1508, using a Honeywell galvanometer, M-40-350A, recorded the free vibration response of the specimen tip each time a damping measurement was made by logarithmic decrement. This response signal was provided to the visicorder by the tip accelerometer through the preamplifiers. The damping measurements using logarithmic decrement were all taken at a root stress level of $\sigma_R = 16450$ psi.

Bandwidth

In the bandwidth method, damping is indicated by the width of the

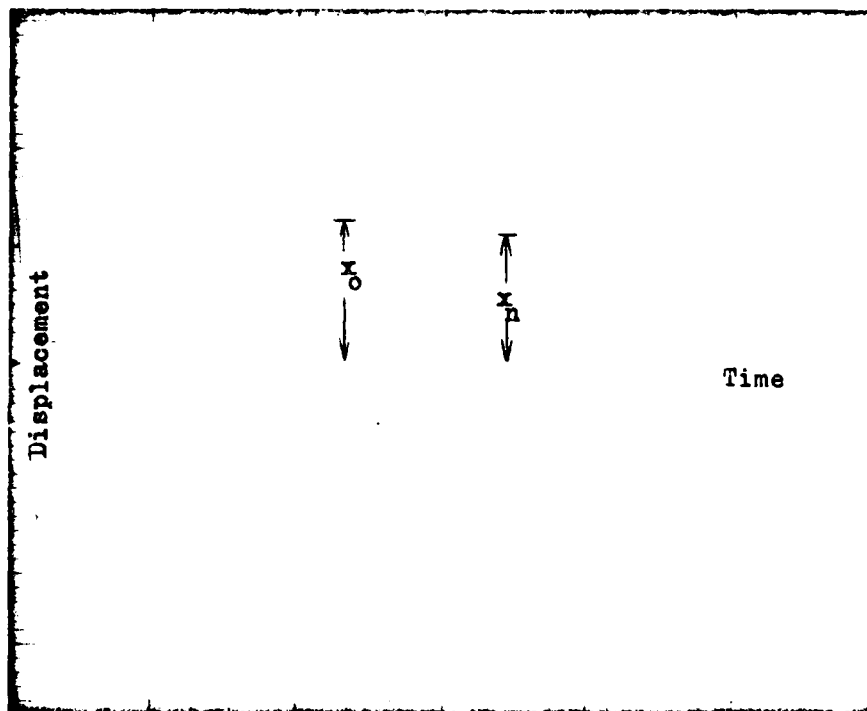


Figure 5. Trace of Damped Free Vibration

response curve near the resonant frequency, ν_R , as shown in Figure 6. Designating the width as a frequency increment, $\Delta\nu$, measured at the half-power points (at a value of $R=R_{\max}/\sqrt{2}$), the damping of the system is defined as $= \frac{\Delta\nu}{2\nu_R}$ for values of $\eta < 0.1$.

The tip accelerometer through the preamplifiers provided a signal to the oscilloscope to monitor the free end response of each specimen. This response was recorded in order to determine damping by the bandwidth method as frequency varied with constant base displacement.

Tables III through XIII illustrate the intervals at which damping measurements were made for each specimen using both bandwidth and logarithmic decrement. Initially, logarithmic decrement only was used to calculate damping. The bandwidth technique was not incorporated until the reading at 10^5 cycles since the specimens had to be vibrated during the bandwidth measurements. At 10^5 cycles and subsequent intervals of measurement, the number of cycles put on the beam during the measurement were negligible compared to the total number of cycles on the beam. Bandwidth damping measurements were taken at a representative root stress level which occurred at the stress level midway between the root stress at the peak response and the root stress at the half-power points of the response curve.

NDT

The Air Force Materials Laboratory performed nondestructive tests on the specimens after the fatigue tests to determine the extent of damage. Radiographic inspection was performed using a Norelco 150 KVP unit. The specimens were treated with tetrabromo-

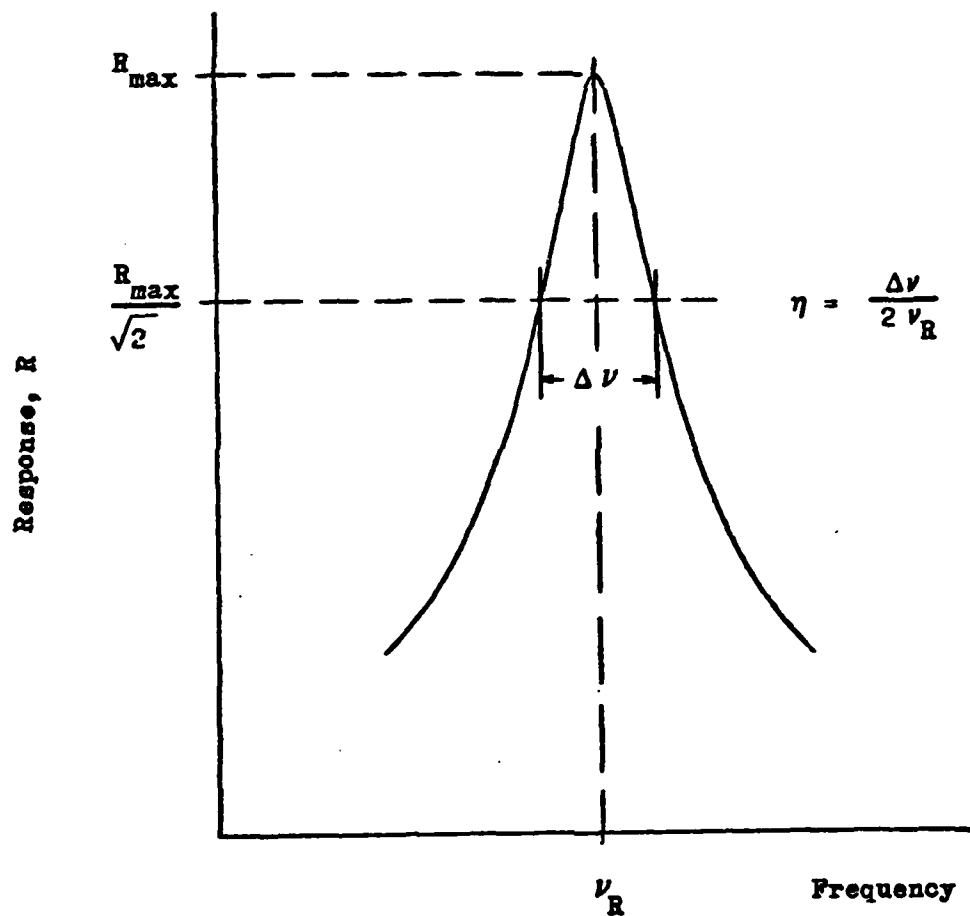


Figure 6. Response Curve Showing Bandwidth
at Half-Power Points

thane on both front and back sides for thirty minutes prior to conducting the x-ray inspection. X-rays were taken at $0, \pm 15$ degrees from the perpendicular.

Ultrasonic C-scans were taken by a Sperry UM 721 Reflectoscope. The ultrasonic frequency range of the instrument amplifier was ten to twenty megahertz. The ultrasonic attenuation of the specimens was four decibels with respect to water.

IV. Results and Discussion

Bending Fatigue

Results of the bending fatigue tests are presented in Table II. The stress, σ_{\max} , is the stress computed to exist at the edge of the hole from the observed tip displacement. The fatigue data in terms of maximum root stress have been plotted in the form of an S-N curve in Figure 7. The line drawn through the experimental points represents the best fit by visual means. Tests on specimens AB 96 and AB 98 were terminated due to mechanical failure. AB 70 was not tested due to the extensive damage present prior to the experiment.

Single, continuous longitudinal cracks were observed to initiate at the hole and progress to the root of each specimen. The width of the damage zone was equal to the diameter of the hole. Figures 8 and 9 illustrate damage in three of the beams which was typical of the damage in each of the specimens. Although not presented here, the x-rays taken at ± 15 degrees from the perpendicular indicated that the damage was not limited to the outer layer.

Damping

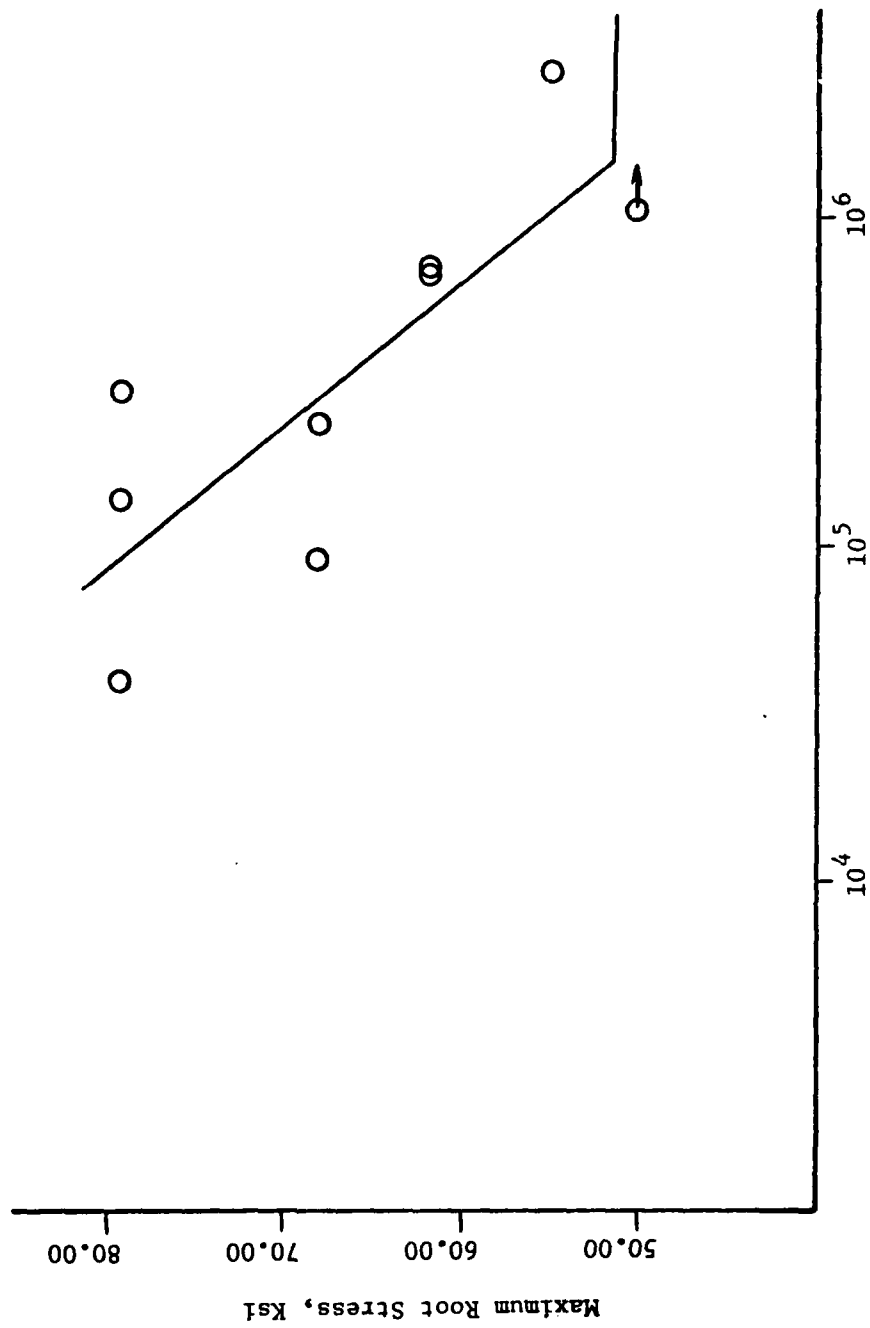
Material damping data were taken at selected cycle increments and calculated from logarithmic decrement and bandwidth. As the number of cycles on each beam increased, the damping increased as expected due to the permanent microstructural damage occurring in the specimens. The damping results show the same general pattern of increase for each specimen regardless of root stress level and total number of cycles applied. Figure 10 typically illustrates how the

Table II

Fatigue Test Results			
Specimen	Maximum Stress at Hole, σ_{\max} , psi	Root Stress, σ_R , psi	Cycles to Failure
AB 74	47850	50700	1.07×10^6 *
AB 77	51530	54600	6.83×10^5
AB 81	63500	67410	9.63×10^4
AB 82	70120	74660	3.96×10^4
AB 90	74110	78560	3.01×10^5
AB 93	64430	68530	2.39×10^5
AB 94	58150	61840	6.93×10^5
AB 95	75960	80780	1.42×10^5
AB 96**	53430	56830	
AB 98**	53960	57380	
AB 99	51860	55160	2.80×10^6

* Failure not observed; test terminated

** Test terminated due to mechanical failure



Log Base 10 of Cycles to Failure

Figure 7. S-N Plot

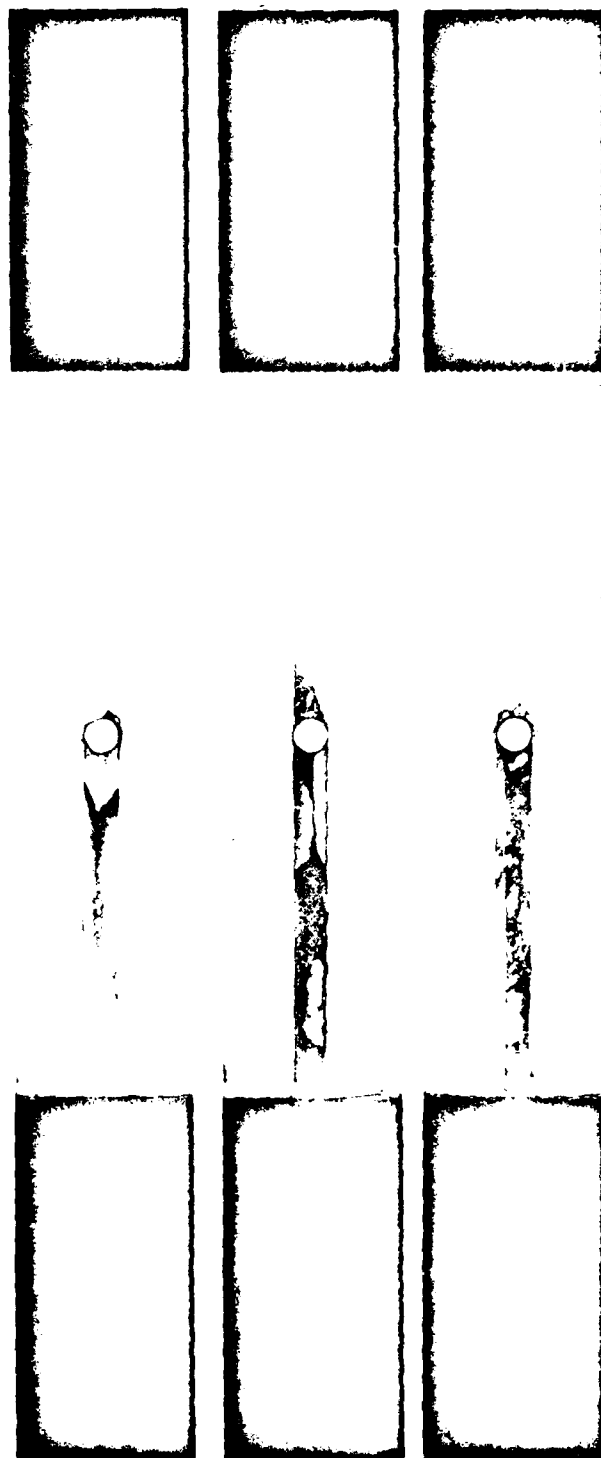


Figure 8. X-rays of Typical Failure

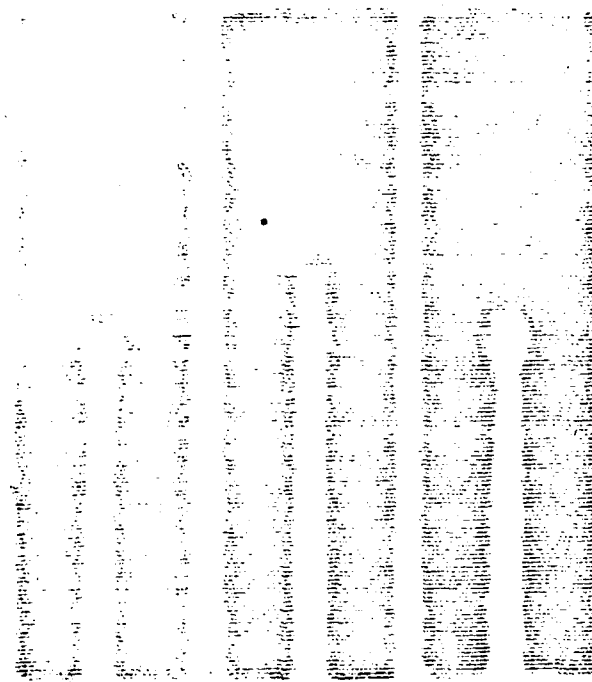
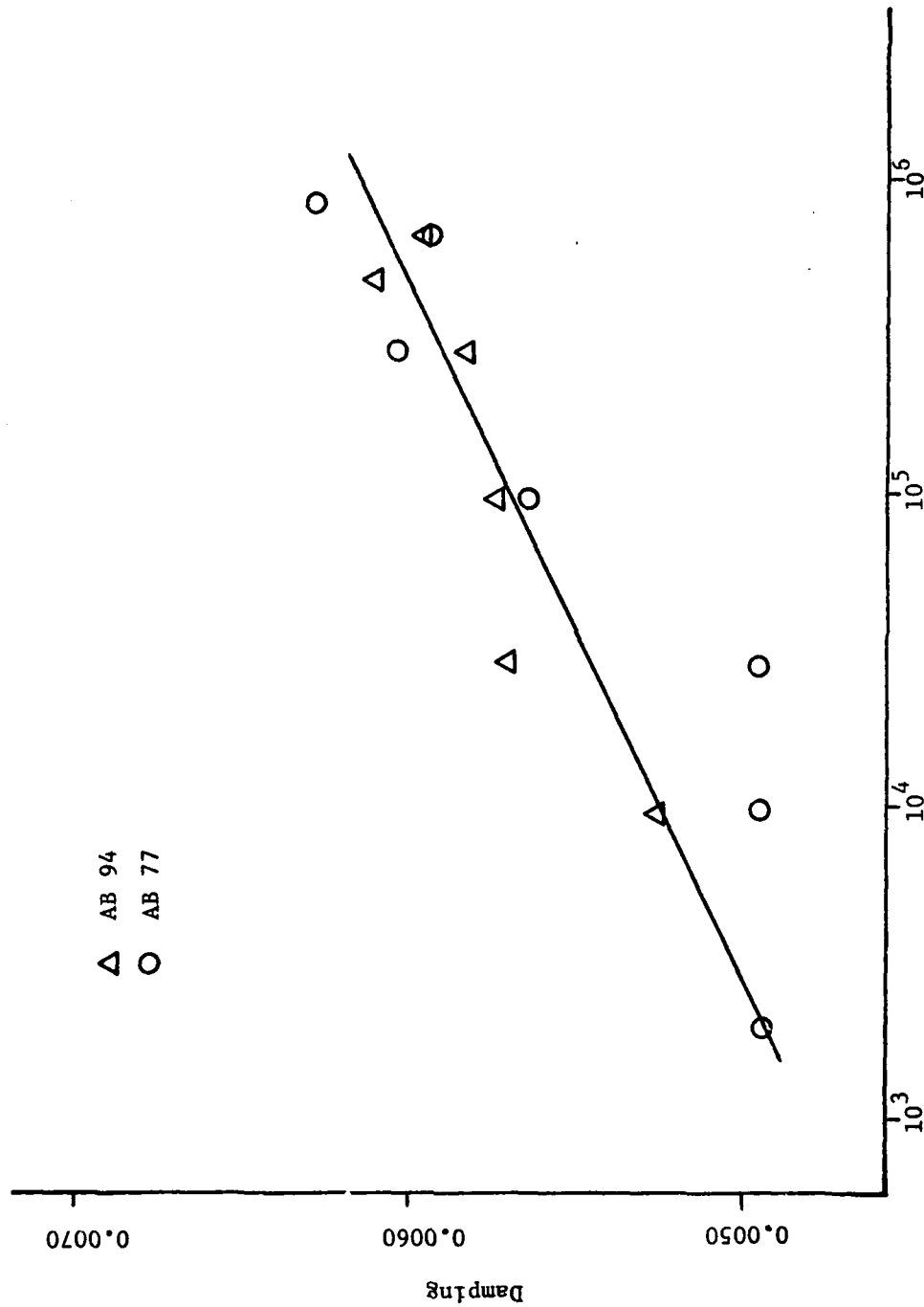


Figure 9. Ultrasonic C-scans of Typical Failure



Log Base 10 of Cycles to Failure
 Figure 10. η -N Plot at Constant Root Stress, $\sigma_R = 61710$ psi

damping changed as the number of cycles increased. Each damping value plotted was calculated by logarithmic decrement at the same stress level, $\sigma_R = 16450$ psi. Logarithmic decrement and bandwidth damping values for all the beams are tabulated in Tables III through XIII. The values in parentheses next to bandwidth in these tables are root stresses in psi at which the bandwidth measurements were made.

An experiment was performed in order to determine how much of the total damping was material damping and how much was air damping. As shown in Figure 11, an aluminum paddle was attached to the free end of one of the specimens, centered on the beam and flush with the tip; the total surface area was increased by a factor of two. Free vibration measurements were taken of the beam by itself and then of the beam with the paddle. Air damping was determined as explained in Appendix C. Results show that air damping was present but was only on the order of five percent of the total damping. Therefore, the damping results are primarily indicative of material damping behavior.

In general, the bandwidth and logarithmic decrement damping values were in fair agreement. This may be due to taking damping measurements at different stress levels; bandwidth measurements were higher and taken at higher stress levels than those measured by logarithmic decrement.

For each logarithmic decrement curve obtained, damping values varied as the stress decreased while the beam damped out in free vibration.

Damping calculated by logarithmic decrement increased as a greater root stress was applied at the same number of cycles.

Table III

Specimen AB74 $\sigma_R = 50700$ psi

Rel Hum = 55%

T = 74°F

N	Log Dec	Bandwidth(38730)
0	.0035	
10^5		.00547
10^6	.00493	.00996

Table IV

Specimen AB77 $\sigma_R = 54600$ psi

Rel Hum = 52%

T = 74°F

N	Log Dec	Bandwidth(50170)
0	.00424	
10^4	.00494	
3×10^4	.00494	
10^5	.00563	.00677
3×10^5	.00602	.00714
6.83×10^5	.00593	.00604
8.73×10^5	.00627	

Table V

Specimen AB81 $\sigma_R = 67410$ psi Rel Hum = 52% T = 74°F

N	Log Dec	Bandwidth(56330)
0	.00420	
10^4	.00426	
3×10^4	.00565	
9.63×10^4	.00541	.00660

Table VI

Specimen AB82 $\sigma_R = 74660$ psi Rel Hum = 54% T = 67°F

N	Log Dec	Bandwidth(64250)
0	.00270	
10^4	.00561	
3.96×10^4	.00605	.00471

Table VII

Specimen AB90	$\sigma_R = 78560$ psi	Rel Hum = 50%	T = 63°F
N	Log Dec	Bandwidth(63370)	
0	.00379		
10^4	.00542		
3×10^4	.00553		
2.52×10^5	.00735		
3.01×10^5	.00710	.00823	

Table VIII

Specimen AB93	$\sigma_R = 68530$ psi	Rel Hum = 45%	T = 82°F
N	Log Dec	Bandwidth(57210)	
0	.00350		
10^4	.00509		
3×10^4	.00515		
10^5	.00511		
2.39×10^5	.00602	.00567	

Table IX

Specimen AB94	$\sigma_R = 61840$ psi	Rel Hum = 47%	T = 70°F
N	Log Dec	Bandwidth(49290)	
0	.00429		
10^4	.00525		
3×10^4	.00570		
10^5	.00572		
3×10^5	.00582	.00529	
5.01×10^5	.00619	.00730	
6.93×10^5	.00595	.00846	

Table X

Specimen AB95	$\sigma_R = 80780$ psi	Rel Hum = 43%	T = 76°F
N	Log Dec	Bandwidth(66890)	
0	.00443		
10^4	.00651		
3×10^4	.00689		
1.42×10^5	.00710	.00680	

Table XI

Specimen AB96 $\sigma_R = 6830$ psi Rel Hum = 44% T = 75°F

N	Log Dec
0	.00441
10^4	.00591
3×10^4	.00587

Table XII

Specimen AB98 $\sigma_R = 57380$ psi Rel Hum = 41% T = 74°F

N	Log Dec
0	.00443
10^4	.00516
3×10^4	.00523
10^5	.00526

Table XIII

Specimen AB99

$\sigma_R = 51860$ psi

Rel Hum = 40%

T = 81°F

N	Log Dec	Bandwidth(42250)
0	.00468	
10^4	.00510	
3×10^4	.00559	
10^5	.00590	.00614
3×10^5	.00580	.00688
10^6	.00596	.00522
2×10^6	.00572	.00522
2.80×10^6	.00580	.00522

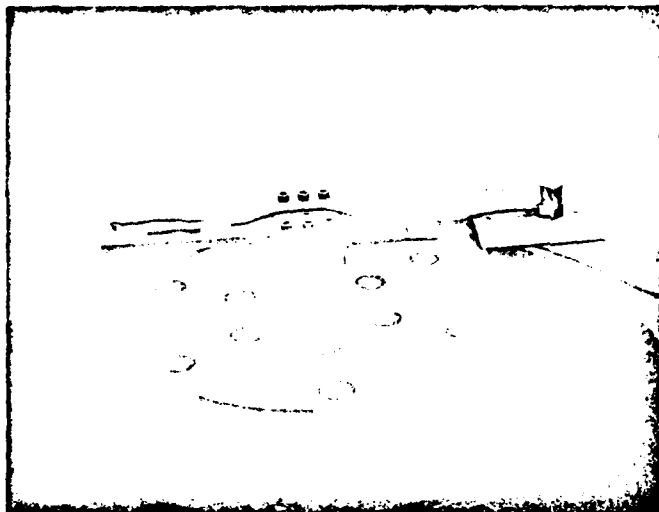
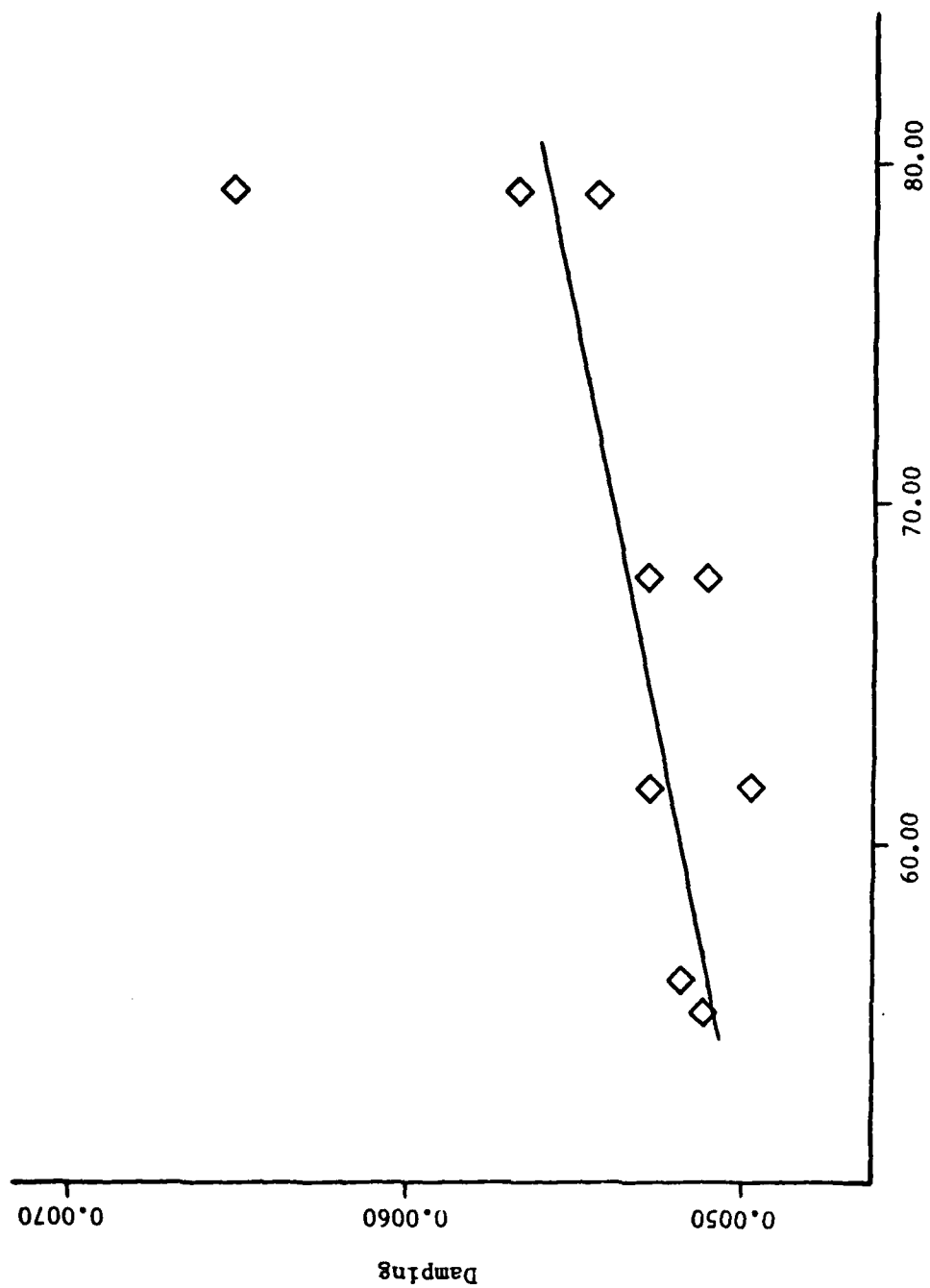


Figure 11. Air Damping Experiment

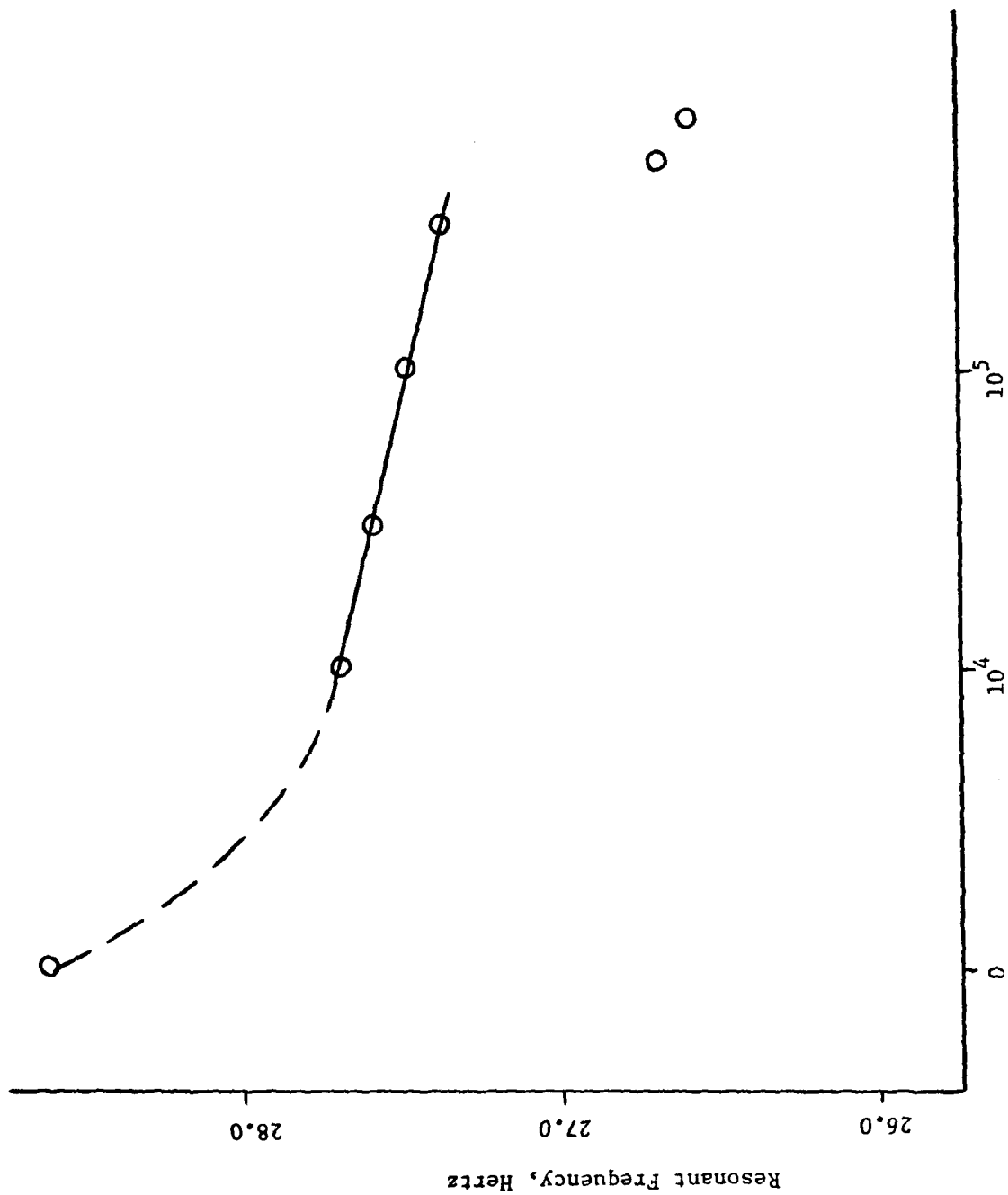
Figure 12 exhibits typical results of the damping increase with increase in root stress. The same results occurred for each cycle increment at which damping was measured.

Frequency

For each specimen, the initial resonant frequency dropped to a lower resonant frequency within 3×10^3 cycles. Resonance occurred at succeeding lower frequencies throughout the test runs. Typically, the final resonant frequency was no more than three cycles less than the initial value as shown in Figure 13 and Table XIV. This decrease is due, as is the damping increase, to the permanent damage experienced by the specimens. Since frequency is a measure of stiffness, this reduction indicates a permanent change in the stiffness of the material.



Root Stress, Ksi
Figure 12. $\eta-\sigma_R$ at 10^4 Cycles



Log Base 10 of Cycles to Failure
Figure 13. N_r -N Plot, Specimen AB 94

Table XIV

<u>Natural Frequency, CPS</u>					
<u>Specimen</u>	<u>0 Cycles</u>	<u>10⁴ Cycles</u>	<u>10⁵ Cycles</u>	<u>10⁶ Cycles</u>	<u>At Failure</u>
AB 74	26.1		25.6	25.6	*
AB 77	27.5	26.8	26.6		25.9
AB 81	28.2	27.3			26.6
AB 82	27.9	26.7			25.6
AB 90	26.6	25.9	25.6		24.9
AB 93	27.0	26.2	25.8		24.7
AB 94	28.6	27.7	27.6		26.6
AB 95	27.8	26.8	25.6		25.0
AB 96	28.3	27.4			**
AB 98	26.9	26.1	26.0		**
AB 99	28.5	27.9	27.7	26.8	26.8,

* Test terminated; no failure observed

** Test terminated due to mechanical failure

V. Conclusions

It is concluded that:

- 1) Test results indicate that it is feasible to quantify damage in composites in terms of changes in material damping; material damping increased as damage occurred in the graphite-epoxy specimens.
- 2) Frequency decreases as damage increases. This a measure of the material stiffness which may also prove to be a valid measure of damage.
- 3) Measured material damping is dependent on stress level; higher stresses yield large damping values.
- 4) Air damping, though present, was not a significant portion of the measured damping. Therefore, the damping values reflect a true change in the material damping.

Bibliography

1. Archie, C. E. The Effects of Thermal Treatments on the Material Damping and Fatigue Properties of 2024 Aluminum Alloy. MS Thesis. Wright-Patterson AFB, Ohio: Air Force Institute of Technology, March, 1966.
2. Ashton, J. E., J. C. Halpin, and P. H. Petit. Primer on Composite Materials: Analysis. Connecticut: Technomic Publishing Company, Inc., 1969.
3. Gibson, R. F. and R. Plunkett. "A Forced-vibration Technique for Measurement of Material Damping," Experimental Mechanics, August 1977.
4. Gibson, R. F. and R. Plunkett. "Dynamic Stiffness and Damping of Fiber-Reinforced Composite Materials," Shock and Vibration Digest, 9(2): 9-17 (February 1977).
5. Gray, T. D. Damage Interaction in Composites. MS Thesis. Wright-Patterson AFB, Ohio: Air Force Institute of Technology. June 1973.
6. Jensen, J. H. The Effects of Thermal Treatments on the Material Damping and Fatigue Properties of 2024 Aluminum. MS Thesis. Wright-Patterson AFB, Ohio: Air Force Institute of Technology, March 1965.
7. Jones, R. M. Mechanics of Composite Materials. Washington, D. C.: Scripta Book Company, 1975.
8. Mazza, L. T., E. B. Paxson, and R. L. Rodgers. "Measurement of Damping Coefficients and Dynamic Modulus of Fiber Composites," USAAVLABS Technical Note 2 (February 1970).

9. Meirovitch, L. Elements of Vibration Analysis. New York: McGraw-Hill Book Company, 1975.
10. Nevadunsky, J. "Fatigue Damage Behavior in Composite Materials," AD A001944, United Aircraft Corporation (September 1974).
11. Nevadunsky, J., J. J. Lucas, and M. J. Salkind. "Early Fatigue Damage Detection in Composite Materials," Journal of Composite Materials, 9: 394-408 (October 1975).
12. Roark, R. J. and W. C. Young. Formulas for Stress and Strain (Fifth Edition). New York: McGraw-Hill Book Company, 1975.
13. Salkind, M. J. "Fatigue of Composites," Composite Materials: Testing and Design (Second Conference). ASTM STP497, American Society for Testing and Materials: 143-169 (1972).
14. Schultz, A. B. and S. W. Tsai. "Dynamic Moduli and Damping Ratios in Fiber-Reinforced Composites," Journal of Composite Materials, 2(3): 368-379 (July 1968).
15. Sendekyj, G. P. and H. D. Stalnaker. "Effect of Time at Load on Fatigue Response of $((0/\pm 45/90)_s)_2$ T300/5208 Graphite-Epoxy Laminate," Special Technical Publication 617, American Society for Testing and Materials, 1977.
16. Timoshenko, S. Vibration Problems in Engineering (Third Edition). New Jersey: D. Van Nostrand Company, Inc., 1966.
17. Tsai, S. W., J. C. Halpin, and N. J. Pagano. Composite Materials Workshop. Connecticut: Technomic Publishing Company, Inc., 1968.
18. Witt, W. P. A Numerical Analysis of Fracture in a Laminated Fibrous Composite Plate. MS Thesis. Wright-Patterson AFB, Ohio: Air Force Institute of Technology, December 1977.

Appendix A

Development of the Composite Stiffness

In order to determine the stiffness of the composite, it is necessary to use the moment equation:

$$M_x = \int_{-c}^c \sigma_x z dx$$

where M_x is the moment per unit length as shown in Figure A-1 and σ_x can be expressed in terms of the laminate middle surface strains, ϵ_x^0 , and curvatures, κ_x

$$\sigma_x = \left[\bar{Q}_{11} \right]_k \left\{ \epsilon_x^0 \right\} + z \left\{ \kappa_x \right\}$$

Then the moment can be written in terms of this stress-strain relationship:

$$M_x = \sum_{k=1}^N \left[\bar{Q}_{11} \right]_k \left(\int_{z_{k-1}}^{z_k} \left\{ \epsilon_x^0 \right\} z dz + \int_{z_{k-1}}^{z_k} \left\{ \kappa_x \right\} z^2 dz \right)$$

where Q_{ij} are transformed reduced stiffnesses and z_k, z_{k-1} are defined in Figure A-2. Since ϵ_x^0 and κ_x are not functions of z but are middle surface values, they can be removed from under the summation sign.

Then this equation can be written as

$$M_x = \left[B_{11} \right] \left\{ \epsilon_x^0 \right\} + \left[D_{11} \right] \left\{ \kappa_x \right\}$$

where $B_{1j} = \frac{1}{2} \sum_{k=1}^N (\bar{Q}_{1j})_k (z_k^2 - z_{k-1}^2)$ and

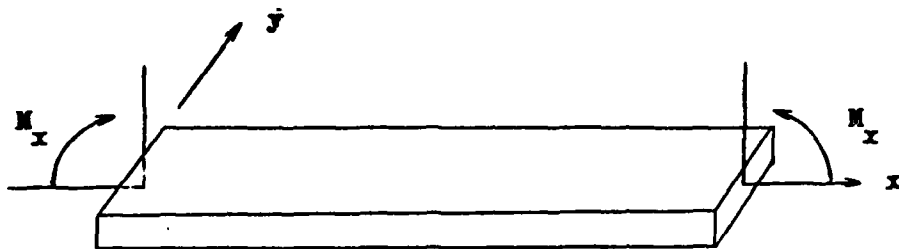


Figure A-1. Moment on Laminate Beam

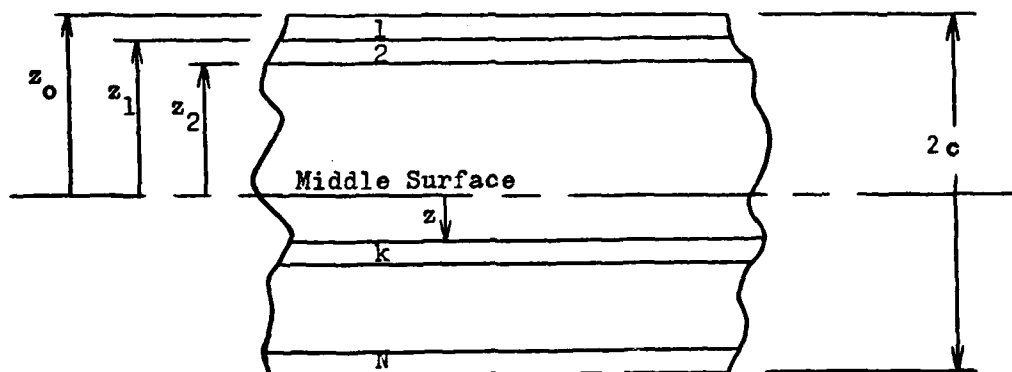


Figure A-2. Geometry of an N-layered Laminate

$$D_{ij} = \frac{1}{3} \sum_{k=1}^N (\bar{Q}_{ij})_k (z_k^3 - z_{k-1}^3)$$

D_{ij} are the bending stiffnesses and B_{ij} are the coupling stiffnesses and imply coupling between laminate bending and extension. Therefore since the beams are assumed to undergo only bending, all $B_{ij} = 0$. Then the moment equation becomes

$$M_x = [D_{11}] \{ \kappa_x \}$$

$$\text{where } D_{11} = \frac{1}{3} \sum_{k=1}^N (\bar{Q}_{11})_k (z_k^3 - z_{k-1}^3)$$

The engineering constants for the beams are

$$E_{11} = 2.3 \times 10^7 \text{ psi}$$

$$E_2 = 1.6 \times 10^6 \text{ psi}$$

$$G_{12} = (.7-.8) \times 10^6 \text{ psi}$$

$$\nu_{12} = .3$$

$$\nu_{21} = .01$$

Then the reduced stiffnesses become

$$Q_{11} = \frac{E_1}{1 - \nu_{12} \nu_{21}} = 2.3069 \times 10^7 \text{ psi}$$

$$Q_{12} = \frac{\nu_{12} E_2}{1 - \nu_{12} \nu_{21}} = 4.8144 \times 10^5 \text{ psi}$$

$$Q_{22} = \frac{E_2}{1 - \nu_{12} \nu_{21}} = 1.6048 \times 10^6 \text{ psi}$$

$$Q_{66} = G_{12} = .75 \times 10^6 \text{ psi}$$

Only one transformed reduced stiffness, \bar{Q}_{11} , is needed to calculate the stiffness. It is related to the reduced stiffness in the following manner:

$$\bar{Q}_{11} = Q_{11} \cos^4 \theta + 2(Q_{12} + 2Q_{66}) \sin^2 \theta \cos^2 \theta + Q_{22} \sin^4 \theta$$

where θ = angle from the x-axis to the axis the fibers are directed along.

$$\text{For the 0 degree plies, } \bar{Q}_{11} = 2.3069 \times 10^7 \text{ psi .}$$

$$\text{For the } \pm 45 \text{ degree plies, } \bar{Q}_{11} = 7.1592 \times 10^6 \text{ psi .}$$

$$\text{For the 90 degree plies, } \bar{Q}_{11} = 1.6048 \times 10^6 \text{ psi .}$$

$$\text{Then } D_{11} = 5.8233 \times 10^2 \text{ lb-in}^2 \text{ .}$$

$$\text{Since } M_x = EI \frac{\partial^2 w}{\partial x^2} = EI \kappa_x \text{ then}$$

$$EI \kappa_x = D_{11} \kappa_x \text{ or } EI = D_{11}$$

$$\text{and } EI = 5.8233 \times 10^2 \text{ lb-in}^2 \text{ .}$$

$$\text{For a beam, the moment of inertia is } I = \frac{bh^3}{12} \text{ .}$$

Using the typical dimensions $b = 1$ inch and $h = .085$ inch for

these specimens, $I = 5.1177 \times 10^{-5} \text{ in}^4$.

The effective Young's Modulus becomes $E = 1.138 \times 10^7 \text{ psi}$
for this composite.

Appendix B

Material Stiffness

In order to verify the calculation of stiffness for the composite specimens, an attempt was made to measure the stiffness experimentally.

Weights were suspended from the free end of a cantilevered specimen and the tip deflection was recorded. The stiffness was then calculated from

$$\delta_T = \frac{Pl^3}{3EI}$$

where P = force applied at distance, l, from the root. Results are presented in Table XV.

Table XV

Static Stiffness

P, lb	δ_T , in Measured	EI, lb-in
.5	.06	378.83
1.0	.12	378.83
1.5	.18	378.83
2.0	.24	378.83

The measured values are in poor agreement with the computed value of EI = 582.33 lb-in. In view of the fact that the computed stiffness led

to a predicted resonant frequency of $\nu_R = 27.85$ cps which was in much better agreement with measured values (26.1 - 28.6 cps) than the value of $\nu_R = 20.42$ cps calculated using Eq (9a) and the measured stiffness, the computed EI was accepted as being correct.

Appendix C

In order to determine how much of the total damping was air damping, an aluminum paddle, three inches square, was attached to a specimen, centered and flush with its tip. This increased the surface area by a factor of two. Free vibration measurements were made of the beam with the paddle and of the beam alone. The resonant frequency was approximately the same for both configurations.

Air damping is proportional to the area of the vibrating object and the square of the maximum amplitude. Linearizing the mode shapes of both configurations led to approximating the air damping in terms of an average amplitude. For the beam alone, expressed in terms of the tip amplitude, this was $0.5\delta_T$. For the beam and paddle, the average amplitude was $0.8\delta_T$. This yielded a damping value for the beam and paddle system six times that of the beam alone.

The measured damping was greater for the beam and paddle than for the beam. Assuming material damping was the same for both cases, it was eliminated from the difference of the two measured values and the air damping was solved for. The air damping was on the order of five percent of the total damping of the beam. Therefore, the damping results in this study are indicative of material damping behavior.

Vita

Cynthia Ann Bourne was born on 8 January 1955 at Fort Sill, Oklahoma. She graduated from George C. Marshall High School in Falls Church, Virginia in 1973 and attended the University of Washington from which she received the degree of Bachelor of Science in Aeronautics and Astronautics. Upon graduation, she received a commission in the United States Air Force through the ROTC program. Upon entering active duty in September 1977, she was assigned to the School of Engineering, Air Force Institute of Technology. Her next assignment is to the Division of Flight Engineering, Air Force Flight Test Center, Edwards AFB, California.

Permanent Address: Route 1
 Sprague, Washington 99032

REPORT DOCUMENTATION PAGE		READ INSTRUCTIONS BEFORE COMPLETING FORM
1. REPORT NUMBER AFIT/GA/AA/78D-2	2. GOVT ACCESSION NO.	3. RECIPIENT'S CATALOG NUMBER
4. TITLE (and Subtitle) MATERIAL DAMPING AS A MEANS OF QUANTIFYING FATIGUE DAMAGE IN COMPOSITES		5. TYPE OF REPORT & PERIOD COVERED MS Thesis
		6. PERFORMING ORG. REPORT NUMBER
7. AUTHOR(s) Cynthia A. Bourne Second Lieutenant		8. CONTRACT OR GRANT NUMBER(s)
9. PERFORMING ORGANIZATION NAME AND ADDRESS Air Force Institute of Technology (AFIT/EN) Wright-Patterson AFB, Ohio 45433		10. PROGRAM ELEMENT, PROJECT, TASK AREA & WORK UNIT NUMBERS
11. CONTROLLING OFFICE NAME AND ADDRESS Air Force Flight Dynamics Laboratory Wright-Patterson AFB, Ohio 45433		12. REPORT DATE December 1978
		13. NUMBER OF PAGES 57
14. MONITORING AGENCY NAME & ADDRESS (if different from Controlling Office)		15. SECURITY CLASS. (of this report) Unclassified
		15a. DECLASSIFICATION/DOWNGRADING SCHEDULE
16. DISTRIBUTION STATEMENT (of this Report) Approved for public release; distribution unlimited		
17. DISTRIBUTION STATEMENT (of the abstract entered in Block 20, if different from Report)		
18. SUPPLEMENTARY NOTES Approved for public release; IAW AFR 190-17 JOSEPH P. HIRPS Major, USAF Director of Information		
19. KEY WORDS (Continue on reverse side if necessary and identify by block number) Composite Materials Graphite-Epoxy Bending Fatigue Test Damping Damage Assessment		
20. ABSTRACT (Continue on reverse side if necessary and identify by block number) The purpose of this study was to experimentally investigate the feasibility of quantifying damage in composites in terms of their damping characteristics. Bending fatigue tests were performed on ((0/45/90) _s) ₂ T300/5208 graphite-epoxy composite specimens. Testing was performed by exciting a cantilever beam so as to maintain a constant amplitude at resonance. Results indicate that the amount of damage occurring in this		

✓ composite can be explained in terms of an increase in its material damping. The resonant frequency (stiffness) was found to decrease as the material damage increased.

UNCLASSIFIED